Modulated Aeroacoustics Cabin Noise Under Controlled Unsteady Flow Conditions for Different Vehicle Geometries

Nur Syafiqah Jamaluddin, Nicholas Oettle

Vehicle Efficiency, Jaguar Land Rover
Abbey Road, Whitley, Coventry, CV3 4LF, UK

njamalud@jaguarlandrover.com
noettle@jaguarlandrover.com

Abstract: The unsteady wind conditions encountered by a vehicle whilst driving on the road are different from those typically experienced in the steady-flow wind tunnel development environment. This paper presents an experimental comparison using two large SUV-shaped vehicles to assess the effect of unsteady wind on modulated noise performance across different vehicle architectures. Both vehicles were also examined with a series of non-production geometric modifications to assess their contribution to modulated noise. The vehicle responses to unsteady wind conditions were assessed using a dynamic upstream unsteady flow generated by active side wind generator of the FKFS wind tunnel. The pressure distribution on the front side glass of both vehicles in the straight-ahead position was also examined to identify the differences in aerodynamic interactions with turbulent inflow between the two vehicle models. The results highlight the geometry-dependent factors that influence both sound levels and modulation characteristics perceived in the cabin under unsteady inflow condition. The tested vehicle with a steeper A-pillar and larger mirror exhibited stronger self-induced unsteadiness and broadband modulation. Conversely, the tested vehicle with a shallower A-pillar and smaller mirror, demonstrated greater sensitivity to upstream turbulence with narrower and low-frequency modulation.

Contribution: 2025 FKFS Conference on Vehicle Aerodynamics and Thermal Management
15 – 16 October 2025 | Leinfelden-Echterdingen

1 Introduction

The unsteady wind noise of a large SUV-shaped vehicle and its modulation characteristics has been examined in previous work by the authors [1]. The present study extends that investigation by including a second vehicle with a different geometry. The unsteady wind conditions experienced by a vehicle whilst driving on the road are different to those typically experienced in the steady-flow wind tunnel environment, due to turbulence in the natural wind, moving through the unsteady wakes of other road vehicles and travelling through the stationary wakes generated by roadside obstacles. Various studies have explored this phenomenon, as summarised comprehensively by [2].

The unsteadiness of the natural wind can create fluctuations in both speed and flow direction over the vehicle, which directly affects the separated flow structures around the side glass region [3]. These structures can generate strong aeroacoustic sources near the vehicle occupants, particularly in regions with greater flow separation [4]. The interaction of this unsteadiness with the vehicle surfaces results in temporal variation in the cabin noise, perceived as modulation or 'bluster' by the occupants. Previous studies comparing the impacts of the unsteady on-road environment on wind noise, using road tests, have been published by [5 - 7].

There has been increased interest in the development of controlled approaches to generate unsteadiness of the natural wind environment as experienced by a vehicle, providing improved reproducibility over on-road tests. Active lift-based devices have been shown to be the most capable of generating the levels of unsteadiness and the longer length scales observed on-road [8 - 10]. The FKFS *Swing* system [11] is an example of a full-scale active lift-based system, which is the basis of the present study. This has been shown to reproduce the levels of unsteady wind noise as experienced on-road through dynamic yaw variation up to 10 Hz.

The aeroacoustic response of a vehicle is also strongly influenced by the local geometry that influence the flow field disturbances around it [12]. The A-pillar flow separation region is known for producing a persistent and complex flow structure, generating strong surface pressure fluctuations and broadband noise, particularly under unsteady conditions [13, 14]. The side mirror, often treated as a bluff body, has geometry and placement that significantly affects vortex shedding and its interaction with the A-pillar wake. Modifications, including those such as inner ducts [15], have been shown to reduce sound pressure levels by stabilising flow and suppressing vortex formation near the mirror-pillar interface.

This work presents the use of an experimental approach, following the methodology described in [1], applied to two SUV-shaped vehicles with distinct A-pillar and side mirror geometries. Both interior sound and exterior surface pressure fluctuations were measured to examine the geometry-dependent influences at the receiver location and in the near field, respectively.

2 Experimental Setup

Two large SUVs were tested using the FKFS full-scale aeroacoustic wind tunnel at the University of Stuttgart in Germany. The experimental methodology followed [1] and included a second vehicle with geometric differences, particularly the A-pillar and side mirror. Interior cabin noise data were recorded using HEAD Acoustics HMS IV binaural heads, while surface pressure fluctuations were measured using HBK Type 4949 surface microphones. The surface microphones, mounted on the front-left side glass of both vehicles, a region where local flow structures are sensitive to flow direction.

Figure 1 shows the schematic diagram around the front side glass of both tested vehicles, highlighting key differences in the A-pillar angle and side mirror geometry as viewed from the side and top planes. SUV_a (Figure 1a), previously studied in [1] has a steeper A-pillar angle than SUV_b (Figure 1b), and features a relatively larger side mirror design. The positioning of the side mirrors relative to the side glass also differs between the two vehicles. In SUV_b (blue-shaded mirror in Figure 1c), the mirror forms a nearly parallel flow channel with a uniform throat gap along its length. In contrast, the mirror curvature of SUV_a (grey-shaded mirror in Figure 1c) creates a converging throat gap that narrows into a shorter parallel channel, guiding the airflow slightly inboard. In terms of vehicle glazing, SUV_a is equipped with toughened side glass, while SUV_b features acoustically laminated side glass of similar thickness.

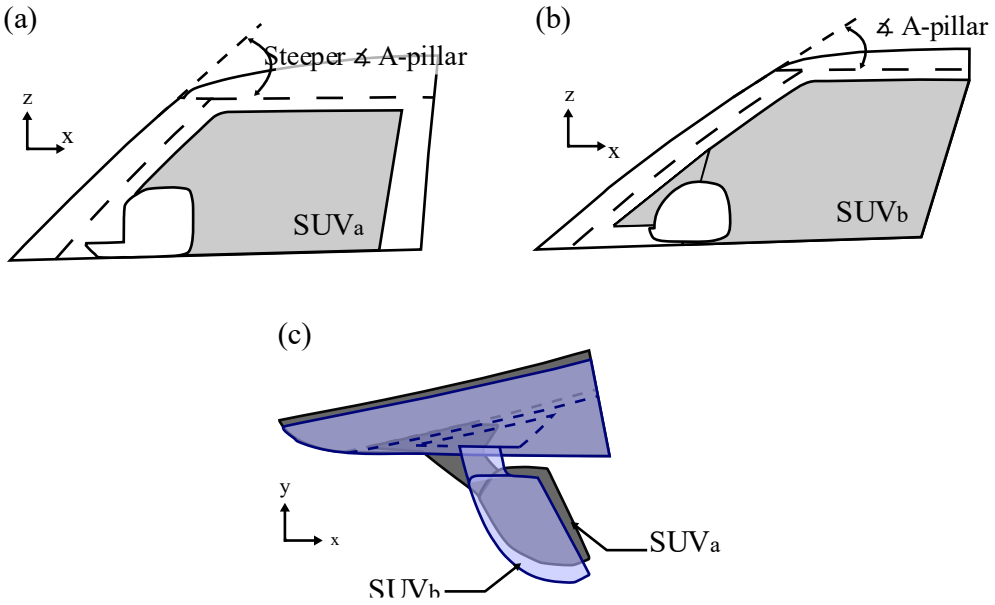

Figure 1: Schematic diagram comparing the front side glass region for (a) SUV_a, and (b) SUV_b, while (c) compares the side mirrors of both vehicles.

Non-production geometry modifications were also investigated by adding a small triangular profile trip along the A-pillar and removing the door mirrors. Tests were conducted at a flow speed of 140 km/h in both steady and unsteady freestream environments with the active side wind generator installed at the nozzle [16]. The unsteady environment is represented by von Kármán 2.5 m (VK) flow conditions, generated synthetically using the von Kármán wind turbulence model [17]. The turbulence characteristics generated are shown in Table 1.

Flow condition	von Kármán 2.5 *m* (VK)
Turbulence length scale	2.5 *m*
Turbulence intensity	6.5 %

Table 1: Turbulence properties of the unsteady flow in lateral direction in an empty test section at 140 km/h.

3 Results and Discussion

3.1 Sound Pressure Level Spectra

This section presents the time-averaged spectral characteristics of both tested vehicles, measured from the front left outer ear (FLOE) in-cabin microphone and surface-mounted microphones along the front-left side glass. Figure 2 presents the interior noise spectra of both vehicles in the fully taped configuration. Results are expressed as ΔSPL_{inflow}, representing the difference in A-weighted sound pressure level (SPL) between steady (SS) and unsteady (VK) inflow conditions. For both vehicles, upstream turbulence increases the spectra within the mid-to-high frequency ranges (1 – 10 kHz).

In SUV_a (Figure 2a), the largest increase occurs above 3 kHz, while changes between 1 and 3 kHz are minimal, likely reflecting excitation from A-pillar and mirror-wake interactions that is less affected by upstream turbulence. For SUV_b (Figure 2b), SPL increases across the spectrum under VK inflow, indicating relatively weaker self-excitation and greater sensitivity to incoming turbulence.

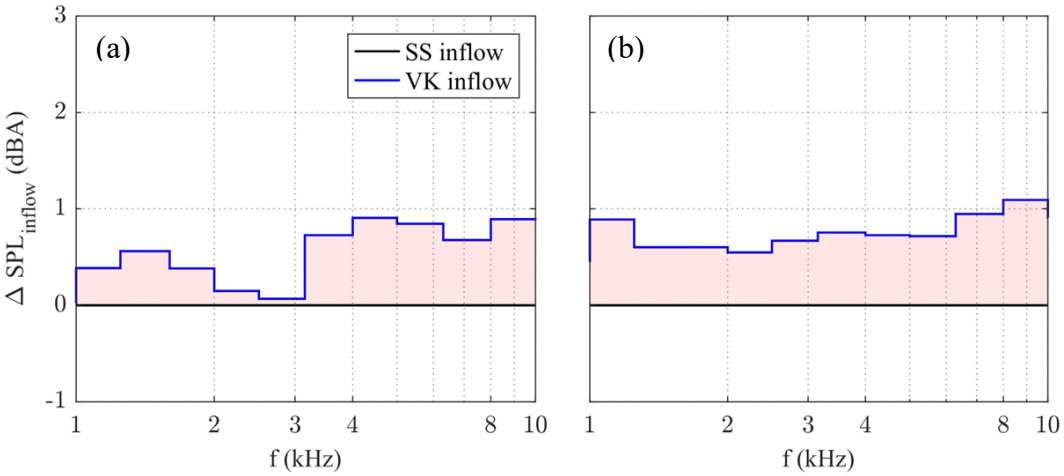

Figure 2: Comparison of interior sound spectra for fully taped (a) SUV_a and (b) SUV_b, shown as the difference in SPL to the steady inflow condition.

To illustrate the flow variation between both vehicles, Figure 3 shows the time-averaged flow topology from CFD simulation of the fully taped vehicles under steady inflow. The simulations were conducted using PowerFLOW and set up following the methodology described in [1, 18]. Results highlight baseline differences in the flow separation regions of the two vehicles. In SUV_a (Figure 3a), the A-pillar vortex appears longer and more developed than in SUV_b. A stronger recirculation is also evident at the mirror-pillar throat region. In addition, the mirror wake of SUV_a is more intense compared to SUV_b (Figure 3b). These flow features reflect the spectral results in Figure 2, where SUV_a indicates a dominant A-pillar and mirror wake interaction compared to SUV_b.

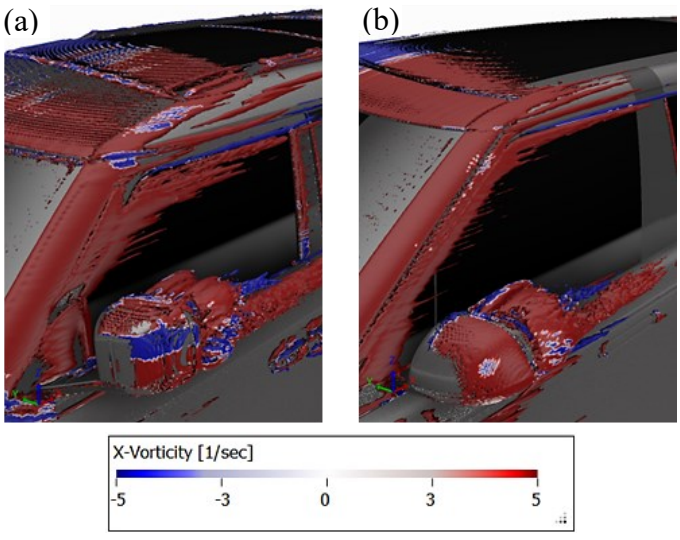

Figure 3: Flow visualisation of (a) SUVa and (b) SUVb in steady inflow conditions.

Figure 4 compares the third-octave spectra for both vehicles with tripped A-pillars and removed side mirrors in turn. Results are presented as the difference in A-weighted SPL between each modified configuration and the fully taped (ΔSPL_{config}), under both inflows. The A-pillar trip cases are shown in red, while the mirror-removed cases are shown in blue. Solid lines denote steady inflow, and dotted lines denote unsteady VK inflow.

In SUV_a (Figure 4a), the tripped A-pillar of increases SPL across the spectra, which has been attributed to trip-induced flow separation that intensifies the A-pillar vortex [1]. Under VK inflow, SPL further increases, likely due to interactions between incoming turbulence and the A-pillar vortex structures. Upstream turbulence may re-energise the separated shear layer or amplify surface pressure fluctuations, increasing the transmitted noise in cabin.

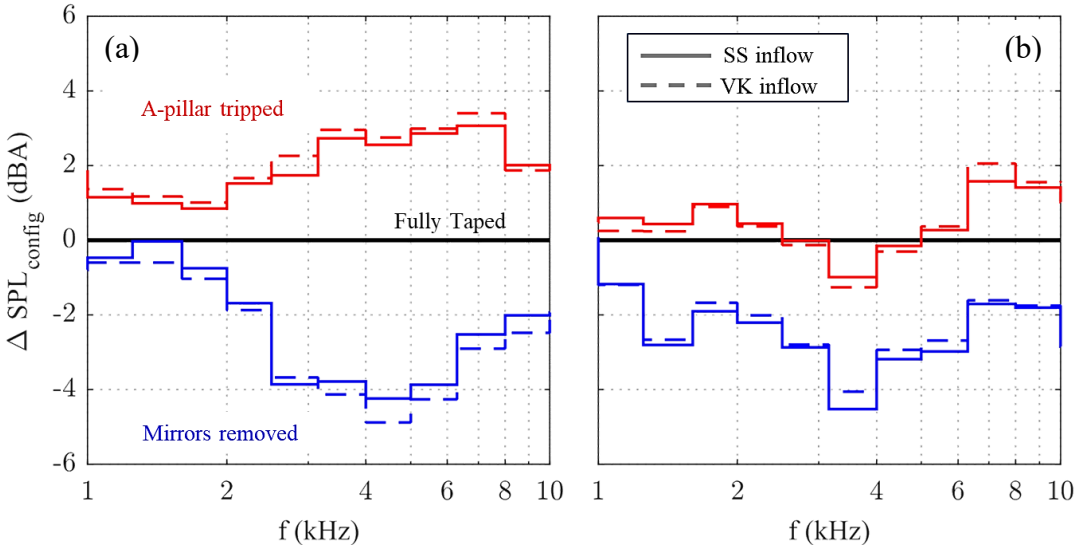

Figure 4: Comparison of interior sound spectra for (a) SUV_a and (b) SUV_b with geometric modifications, shown as the difference in SPL to the fully taped configuration.

For SUV_b (Figure 4b), the tripped A-pillar also increases SPL, albeit to a lesser extent. This is likely due to acoustic lamination of the side glass and a shallower A-pillar angle, which attenuates noise transmission and weakens the separated flow respectively. A local SPL reduction around 3 kHz is observed, possibly linked to modified local flow near front door quarter glass, which reduces excitation in that region.

Removing the side mirrors reduces SPL for both vehicles under all inflow conditions due to the elimination of mirror vortex shedding [1]. In SUV_b (Figure 4b), the mirrors-removed case shows a more broadband SPL reduction than SUV_a (Figure 4a), particularly within the 1 to 2 kHz range. This likely reflects the influence of its geometry and glazing specification. Under VK inflow, SUV_a shows a further SPL decrease, possibly due to breakdown of the remaining A-pillar flow structures without mirrors. In contrast, SUV_b shows a slight increase under VK inflow, suggesting that without mirrors its A-pillar wake is less responsive to upstream turbulence.

Figure 5 presents the surface SPL distribution (ΔSPL_{inflow}) on the front-left side glass of both vehicles for the fully taped, A-pillar tripped, and mirrors removed configurations. These pressure maps provide spatial insights into the nearfield pressure environment, capturing both hydrodynamic and acoustic contributions (albeit dominated by the hydrodynamic fluctuations), and help identify source regions that influencing the noise perceived in cabin.

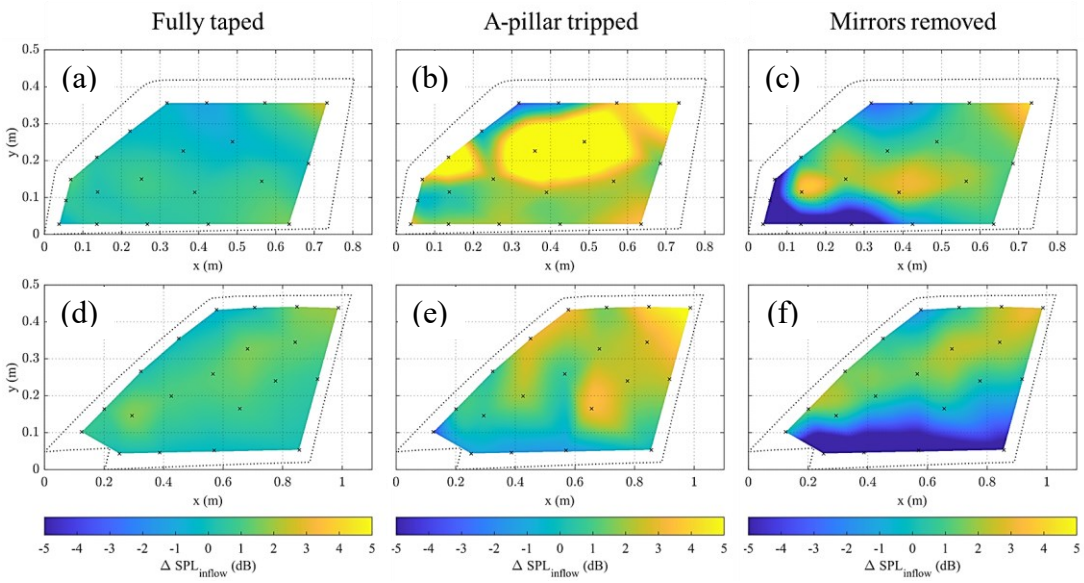

Figure 5: The distribution of surface SPL, expressed in ΔSPLinflow, on the front left side glass of SUVa (a) – (c) and SUVb (d) – (f) in different test conditions.

In the fully taped configuration, both vehicles show a slight increase in surface SPL under VK inflow, but with different distributions. SUV_a (Figure 5a) shows a localised increase downstream of the mirror with little change along the A-pillar, in line with the limited response to turbulence seen in Figure 2. SUV_b (Figure 5d), on the other hand, shows a broad surface SPL increase along the A-pillar wake, consistent with the broadband response seen in the interior sound spectra.

With the A-pillar tripped, SUV_a (Figure 5b) shows a significant increase in surface SPL, localised near the A-pillar and further downstream along the side glass. This trend reflects the interior spectra in Figure 4a, with a stronger vortex shedding at the tripped A-pillar interacting with the upstream turbulence. SUV_b (Figure 5e) also shows an increase in surface SPL, but at relatively lower levels, with a localised reduction near the front quarter glass region, in line with the 3 kHz dip observed in Figure 4b.

When the side mirrors are removed and under VK inflow, both vehicles show reduced surface SPL in the mirror wake region near the bottom of the A-pillar, approximately between 0.5 m < y < 0.15 m. This region represents the area subjected to the wake of the cowl vortex under upstream turbulence, which may interact and break the vehicle's A-pillar vortex structures more effectively without the mirror. For SUV_a (Figure 5c), this surface SPL reduction is localised in the upstream half of the side glass, up to nearly x = 0.4 m. In contrast, this reduction is broader and spanned across the entire length of the side glass for SUV_b (Figure 5f), which is in-line to the broadband decrease in the interior spectra seen in Figure 4b.

3.2 Modulation Spectra

This section presents the modulation characteristics of the tested vehicles under the same test configurations and inflow conditions as previously analysed in Section 3.1. Modulation analysis was conducted using the Hilbert transform to extract the signal's envelope following the method described in [1]. This approach was then extended to isolate the fundamental modulation, as described in [19], and provides the wind-induced modulated noise in terms of its carrier frequency (F_c), degree of modulation (m) and frequency of modulation (F_m).

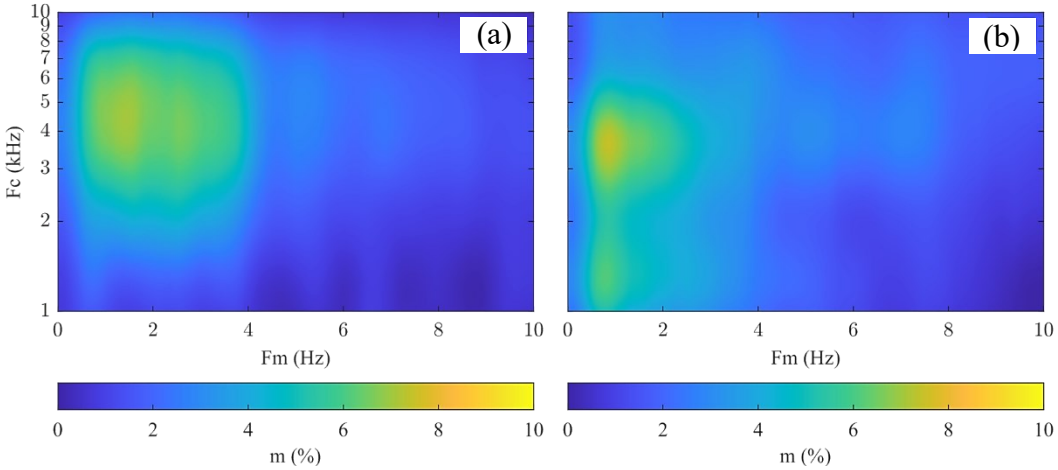

Figure 6: Comparison of wind-induced modulation spectrogram between (a) SUVa and (b) SUVb under unsteady inflow in the fully taped configuration.

Figure 6 compares the wind-induced modulation spectrograms for both tested vehicles in fully taped configuration under unsteady VK inflow. Steady inflow cases show near-zero modulation across all configurations and are not included for brevity. For SUV_a (Figure 6a), a broadband modulation over 5% is observed between 2 to 8 kHz at fluctuation rates of up to 4 Hz. In contrast, SUV_b (Figure 6b), shows a more band-limited response, with over 5% around 4 kHz and modulation frequencies limited to about 2 Hz. These differences are consistent with the geometric differences and flow characteristics described earlier, where SUV_a tends to generate stronger self-induced separation that interacts with upstream turbulence more than SUV_b.

These characteristics can be further examined from the two-dimensional modulation spectra in Figure 7, where the wind-induced modulation contributions of partial octave bands are presented. SUV_a (Figure 7a) shows a broader modulation spread, while SUV_b (Figure 7b) is more band-limited with a distinct peak. In both vehicles, the dominant modulation occurs at 4 kHz with similar levels of about 7%. At other octave bands, SUV_a is characterised by contributions at higher frequencies (i.e. 8 kHz), while SUV_b at lower frequencies (i.e. 1 and 2 kHz).

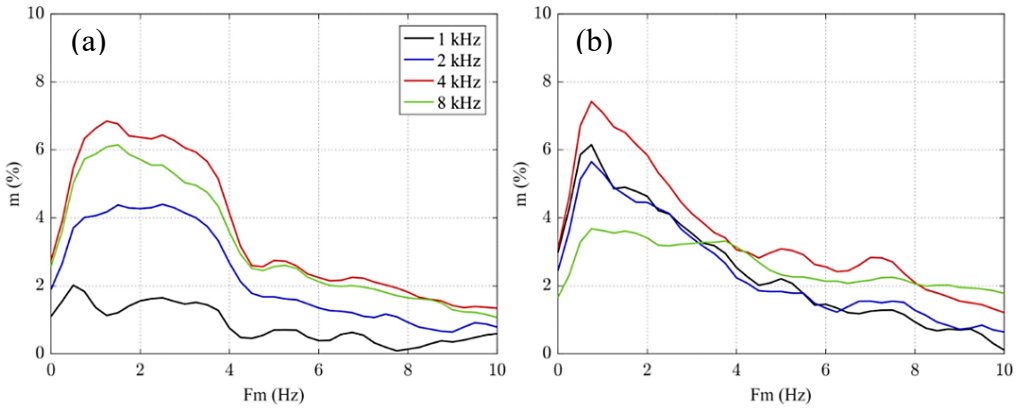

Figure 7: The wind-induced modulation spectra at varying octave band frequencies for (a) SUV_a and (b) SUV_b in the fully taped configuration.

Geometric modifications can further influence the modulation characteristics of both vehicles. This can be clearly demonstrated in Figure 8, where the wind-induced modulation spectrogram of both vehicles under VK inflow at varied test configurations are compared. When the A-pillar is tripped, the airflow is forced to separate earlier and more consistently, generating a stronger vortex compared to the weaker baseline structures without it.

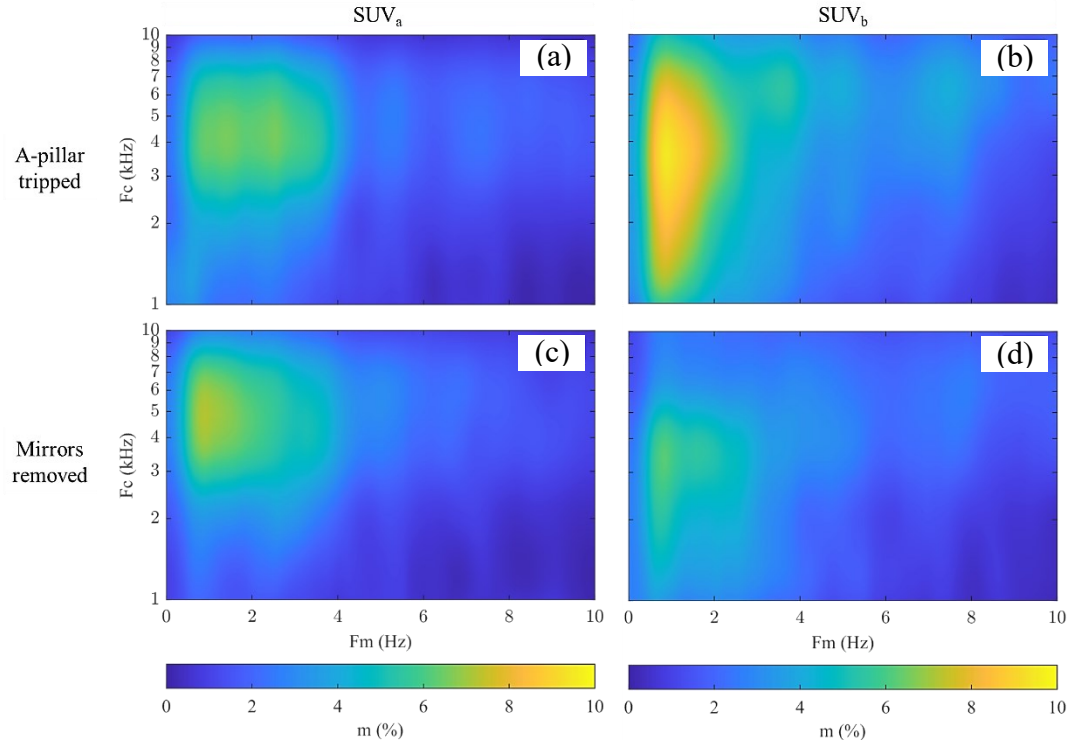

Figure 8: Comparison of wind induced modulation spectrograms for SUV$_a$ ((a) and (c)) and SUV$_b$ ((b) and (d)) for different test configurations.

For SUV$_a$ (Figure 8a), the modulation trends are similar to those seen in fully taped, but at slightly lower levels and band-limited. This can be attributed to its steeper A-pillar that already experience strong baseline A-pillar vortex, which lowers its sensitivity to upstream turbulence and the corresponding modulation characteristics. In contrast, the tripped A-pillar case of SUV$_b$ (Figure 8b) shows significantly higher modulation than untripped, with up to 10% modulation at a rate between 1 to 8 kHz. This may be due to its shallower A-pillar and weaker baseline vortex that gets stronger when tripped and becomes more sensitive to upstream turbulence. The modulation frequency, however, remains limited to about 2 Hz, similar to that observed in fully taped.

With the mirrors removed, the modulation characteristics of SUV$_a$ in Figure 8c remain comparable to the fully taped results, with a slight reduction at rates between 2 to 4 Hz. This trend is similar to Figure 5c, where localised SPL reductions on the side glass are observed together with regions that remain highly responsive to upstream turbulence. For SUV$_b$ (Figure 8d), a broader decrease in modulation is observed, consistent with the trend in Figure 5f, which shows a wider reduction of surface SPL along the side glass.

4 Conclusion

This study compares the aeroacoustic characteristics of two large SUV-shaped vehicles under unsteady inflow, focusing on how differences in geometry influence the perceived noise in cabin. SUV_a, that has steeper A-pillar, larger mirror and converging throat gap, generates stronger self-induced flow structure that dominates the response even under steady-state inflow. In contrast a SUV_b, with its shallower A-pillar, smaller mirror, and laminated side glass, produces quieter baseline noise and weaker flow separation with greater sensitivity to upstream turbulence. These characteristics were consistently observed across the interior spectra, surface pressure distribution and modulation analysis.

The CFD flow topology corroborate this trend with SUV_a showing longer and stronger A-pillar vortices and more intense mirror wakes than SUV_b. Geometric modifications further emphasise the role of baseline flow behaviour, where tripping the A-pillar had shown little effect on SUV_a with its larger vortex but increased SPL and modulation in SUV_b, while mirror removal reduced the mirror-wake contribution in both vehicles, more broadly for SUV_b.

The modulation results provided insight into how these flow features translate into perceived sound quality. SUV_a was characterised by a broadband modulation spread at higher carrier frequencies, which may be masked by the higher levels of overall SPL. SUV_b, on the other hand, showed narrower and more peaky modulation, concentrated at lower octave carrier bands with modulation rates up to 2 Hz, where human hearing is more sensitive. Overall, these findings highlight the geometry-dependent factors that influence both sound levels and modulation characteristics perceived in the cabin.

5 Acknowledgement

The authors wish to thank the staff of the FKFS full-scale aeroacoustic wind tunnel for their assistance during testing, instrumentation and discussion; Oliver Smith and Lucas Padial for supporting the CFD image generation; and to JLR for permission to publish.

6 Reference list

1. N.S. Jamaluddin, N. Oettle, and D. Staron. Experimental Investigation into Modulated Aeroacoustic Cabin Noise Arising from Unsteady Flow Conditions. SAE Technical Paper 2025-01-0029, 2025. doi:10.4271/2025-01-0029.
2. D. Sims-Williams. Cross Winds and Transients: Reality, Simulation and Effects. SAE Int. J. Passeng. Cars - Mech. Syst. 4(1):172–183, 2011. doi:10.4271/2011-01-0172.

3. N. Oettle, D. Sims-Williams, and R. Dominy. Assessing the Aeroacoustic Response of a Vehicle to Transient Flow Conditions from the Perspective of a Vehicle Occupant. SAE Int. J. Passeng. Cars - Mech. Syst. 7(2), 2014. doi:10.4271/2014-01-0591.
4. N. Oettle and D. Sims-Williams. Automotive Aeroacoustics: An Overview. Proc. Inst. Mech. Eng. D: J. Automob. Eng. 231(9):1177–1189, 2017. doi:10.1177/0954407017695147.
5. N. Lindener, H. Miehling, A. Cogotti, F. Cogotti et al. Aeroacoustic Measurements in Turbulent Flow on the Road and in the Wind Tunnel. SAE Technical Paper 2007-01-1551, 2007. doi:10.4271/2007-01-1551.
6. C. Peric, S. Watkins, E. Lindqvist, and J. Saunders. Effects of On-Road Turbulence on Automotive Wind Noise: Comparing Wind-Tunnel and On-Road Tests. SAE Technical Paper 970406, 1997. doi:10.4271/970406.
7. Oettle, N., Mankowski, O., Sims-Williams, D., Dominy, R. et al., "Evaluation of the Aerodynamic and Aeroacoustic Response of a Vehicle to Transient Flow Conditions," SAE Int. J. Passeng. Cars - Mech. Syst. 6(1):2013, doi:10.4271/2013-01-1250.
8. S. Terakado, T. Makihara, T. Sugiyama, K. Maeda et al. Experimental Investigation of Aeroacoustic Cabin Noise in Unsteady Flow by Means of a New Turbulence Generating Device. SAE Int. J. Passeng. Cars - Mech. Syst. 10(1):2017. doi:10.4271/2017-01-1545.
9. D. Staron, M. Riegel, R. Blumrich, and A. Wagner. Aeroacoustic Vehicle Development Method Considering Realistic Wind Conditions. SAE Technical Paper 2023-01-1123, 2023. doi:10.4271/2023-01-1123.
10. O. Mankowski, D. Sims-Williams, and R. Dominy. A Wind Tunnel Simulation Facility for On-Road Transients. SAE Int. J. Passeng. Cars - Mech. Syst. 7(3):2014. doi:10.4271/2014-01-0587.
11. M. Riegel, R. Blumrich, and M. Helfer. New Technology for Unsteady Wind Noise Measurements in an Aeroacoustic Full-Scale Wind Tunnel. Int. Conf. Vehicle Aerodynamics, Coventry, September 21–22, 2016.
12. D. Staron, M. Riegel, R. Blumrich, and J. Wiedemann. Vergleich von Methoden zur Bestimmung des instationären Windgeräuschs im Fahrzeug. Tagung Fahrzeug-Aerodynamik, Haus der Technik, München, 3–4 July 2018. Tagungsschrift Fahrzeugakustik und -schwingungen.
13. J. Howell, J.B. Fuller, and M. Passmore. The effect of free stream turbulence on a-pillar airflow. SAE Technical Paper 2009-01-0003, 2009. doi:10.4271/2009-01-0003.
14. J. Fischer, V. Valeau, L. E. Brizzi, and J. Laumonier. Joint acoustic and wall-pressure measurements on a model A-pillar vortex. Exp. Fluids 61(2):54, 2020. doi:10.1007/s00348-020-2880-5.
15. Y-J. Chu, Y-S. Shin, and S-Y. Lee. Aerodynamic Analysis and Noise-Reducing Design of an Outside Rear View Mirror. Appl. Sci. 8(4):519, 2018. doi:10.3390/app8040519.
16. R. Blumrich, N. Widdecke, J. Wiedemann, A. Michelbach et al. New FKFS Technology at the Full-Scale Aeroacoustic Wind Tunnel of University of Stuttgart. SAE Technical Paper 2015-01-1557, 2015. doi:10.4271/2015-01-1557.
17. F.W. Diederich and J.A. Drischler. Effect of spanwise variations in gust intensity on the lift due to atmospheric turbulence. NACA-TN-3920, 1957.
18. O. Smith and N. Oettle. Visualisation of Roof Bar Noise Sources through the Use of Acoustic Beamforming and Computational Aeroacoustics. SAE Technical Paper 2023-01-0840, 2023. doi:10.4271/2023-01-0840.
19. D. Staron. Entwicklung einer Methode zur Bestimmung und Bewertung des Windgeräuschs im Fahrzeug unter realistischen Strömungsbedingungen. Springer Vieweg, Wiesbaden, 2025.